

Supporting Information

Ion transport, mechanical properties and relaxation dynamics in structural battery electrolytes consisting of an imidazolium protic ionic liquid confined into a methacrylate polymer

Achilleas Pipertzis¹, Nicole Abdou², Johanna Xu³, Leif E. Asp³, Anna Martinelli², Jan Swenson^{1,*}

¹Department of Physics, Chalmers University of Technology, Gothenburg 41296, Sweden.

²Department of Chemistry and Chemical Engineering, Chalmers University of Technology, Gothenburg 41296, Sweden.

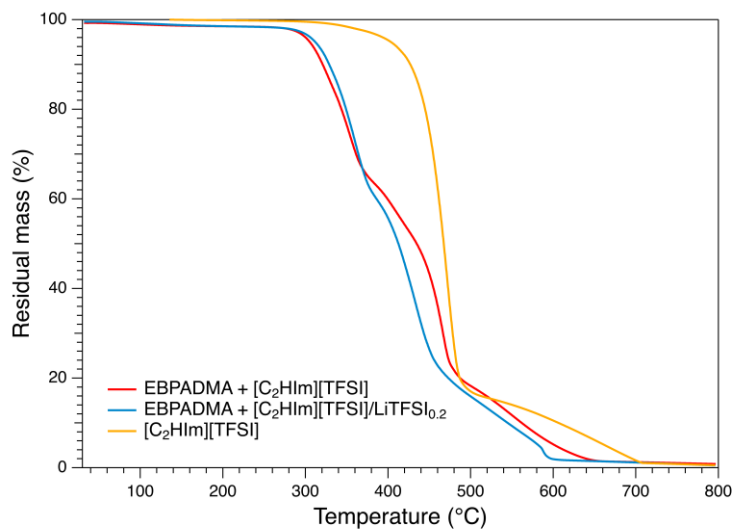
³Department of Industrial and Materials Science, Chalmers University of Technology, Gothenburg 41296, Sweden.

Correspondence to: Prof. Jan Swenson, Department of Physics, Chalmers University of Technology, Gothenburg 41296, Sweden. E-mail: jan.swenson@chalmers.se

Outline

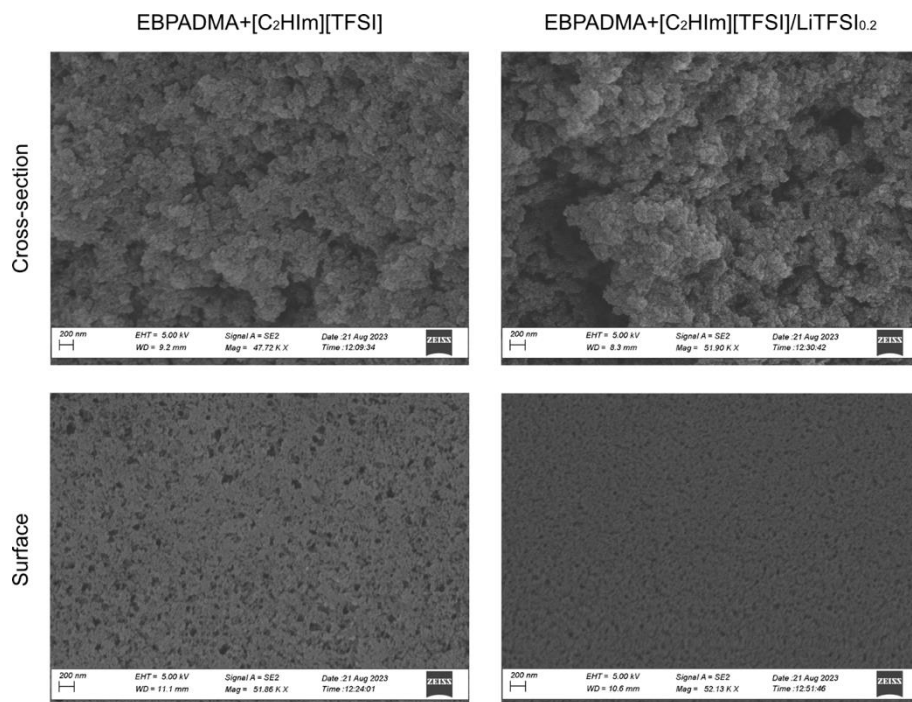
1. Thermogravimetric analysis (TGA) data
2. Scanning electron microscopy (SEM) images
3. Thermodynamic data (TM-DSC)
4. Raman spectroscopy data
5. Dielectric spectroscopy data

1. Thermogravimetric analysis (TGA)



Supplementary Figure 1. Thermograms of the pure ionic liquid (yellow), the ionic liquid confined in the polymer with (blue) and without (red) LiTFSI.

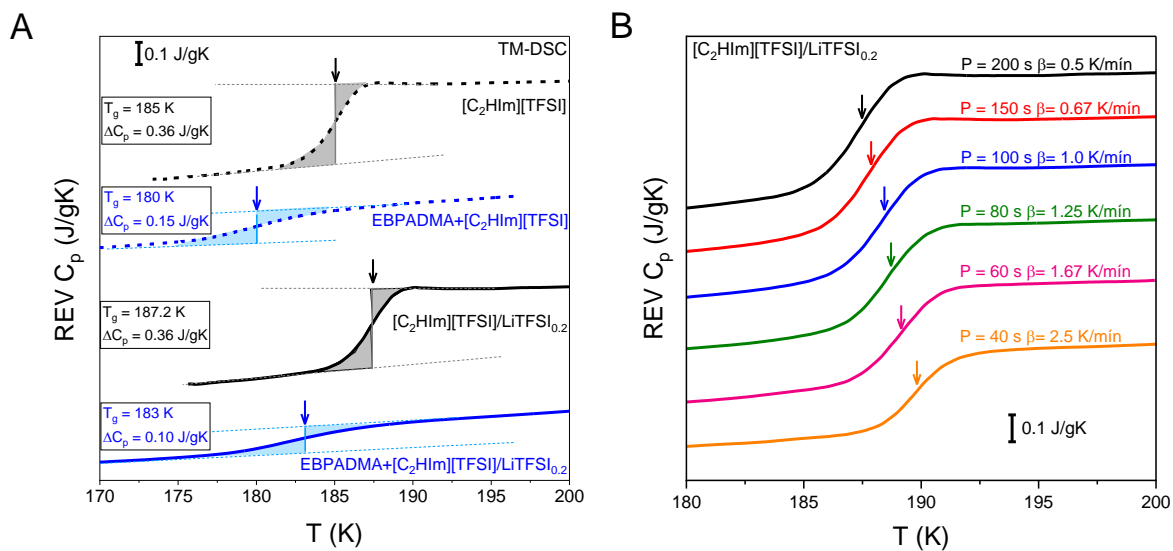
2. Scanning electron microscopy (SEM) images



Supplementary Figure 2. Cross-sectional (top) and surface (bottom) SEM images of EBPADMA+[C₂HIm][TFSI] (left) and EBPADMA+[C₂HIm][TFSI]/LiTFSI_{0.2} (right) samples. Scale bar: 200 nm.

3. Thermodynamic data (TM-DSC and standard DSC)

The effect of confining the protic ionic liquid into the polymer structure on the thermodynamic glass transition temperature (T_g) is shown in **Supplementary Figure 3A**. The change of T_g by altering the period of modulation and the corresponding linear heating rate is also represented in **Supplementary Figure 3B**. The figure shows that T_g decreases by about 4 K upon confinement, implying weak interfacial interaction between the liquid and the solid phases and a strong geometrical confinement effect. The doping with Li-salt increases T_g by about 3 K, reflecting stronger ionic interactions, that increase the liquid's viscosity and thus increases T_g . Furthermore, T_g increases for lower periods of modulation and faster heating rates, reflecting the VFT dependence of the structural relaxation (α -process coupled to σ -process), as shown in **Figure 11** of the main text of the article. In **Supplementary Table 1**, values of the cold-crystallization, the melting and the glass transition temperature are given, together with the enthalpy change of melting, the heat capacity change and the width of the glass transition temperature for the structural electrolytes and their respective bulk liquid phases.



Supplementary Figure 3. (A) Temperature dependence of reversing heat capacity of the methacrylate-based solid electrolytes (blue lines) and their respective bulk liquid electrolytes (black lines) at a Li-salt concentration of 0.0 m (dashed lines) and 0.2 m (solid lines). (B) Reversing heat capacity as a function of temperature for [C₂HIm][TFSI]/LiTFSI_{0.2} at different periods of modulation and corresponding linear heating rates.

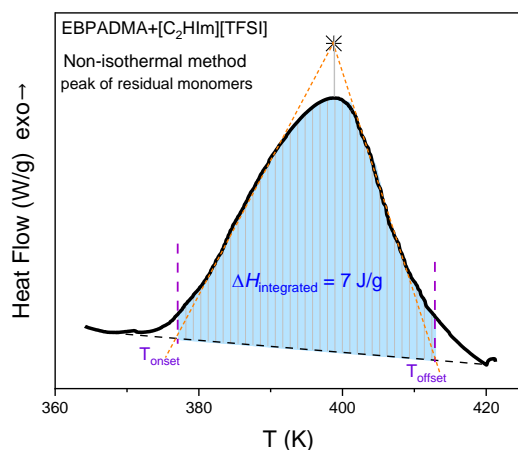
Supplementary Table 1. Cold-crystallization, melting and glass transition temperatures along with the enthalpy change of melting and the change of heat capacity for the methacrylate-based solid electrolytes and their respective liquid electrolytes.

Sample	Crystalline part			Amorphous part				
	T_{cc} (K)	T_m (K)	ΔH_m (J.g ⁻¹)	T_g^{PIL} (K)	ΔC_p (J.g ⁻¹ .K ⁻¹)	ΔT_g^{PIL} (K)	$T_g^{EBPADMA}$ (K)	$\Delta T_g^{EBPADMA}$ (K)
[C ₂ HIm][TFSI]	240.6±0.5	281.6±0.6	71±5	183.9±0.7	0.36	6.0	-	-
[C ₂ HIm][TFSI]/LiTFSI _{0.1}	255.3±0.4	274.5±0.3	35±3	-	-	-	-	-
[C ₂ HIm][TFSI]/LiTFSI _{0.2}	260.3±0.5	274.8±0.4	31±4	187.2±0.6	0.36	4.4	-	-
EBPADMA+[C ₂ HIm][TFSI]	232.0±1.0	272.0±1.0	8±1	180.0±1.0	0.15	9.8	330 ± 10	46
EBPADMA+[C ₂ HIm][TFSI]/LiTFSI _{0.2}	233.0±1.0	267.0±1.0	5±1	183.0±1.0	0.10	9.1	320 ± 10	47

The conversion rate of the EBPADMA polymer can also be calculated from the first heating cycle of the standard DSC, by employing a non-isothermal method, as shown in **Supplementary Figure 4**. During the first heating cycle, the DSC trace exhibits an exothermic peak at 399 K, associated to the polymerization of *residual monomers*. The degree of polymerization can be calculated by employing the following equation¹:

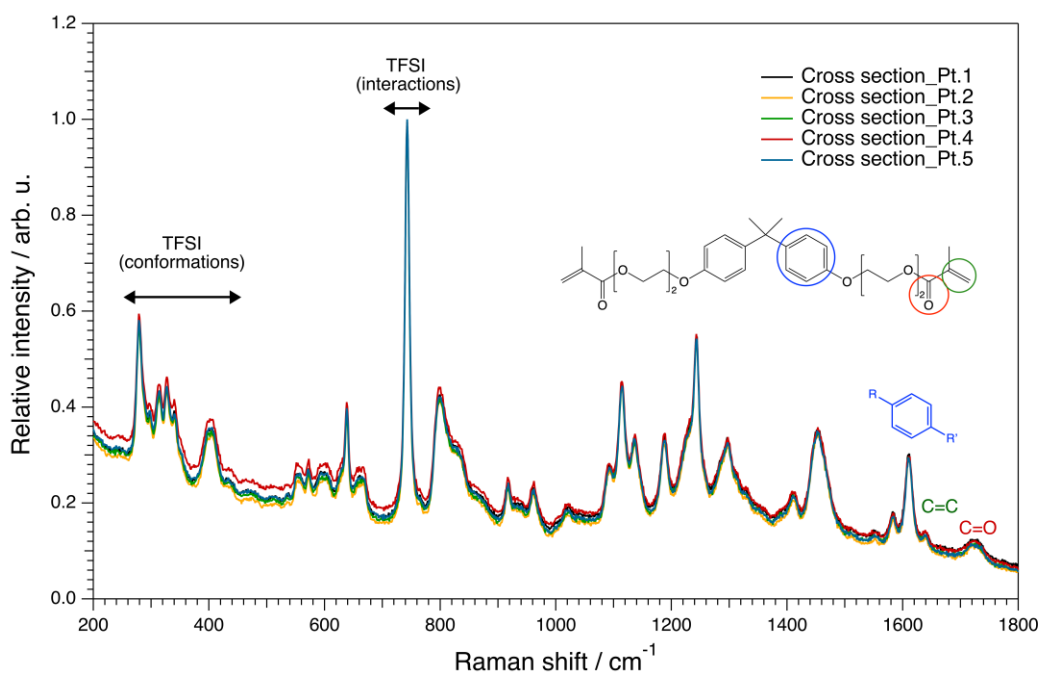
$$DC(\%) = \left[1 - \left(\frac{E_p \cdot M_w}{\Delta H_{pol} \cdot m_a} \right) \right] \times 100 = 94\%$$

where, ΔH_{pol} (= 60 kJ/mol) is the standard enthalpy of polymerization¹, E_p (= $\Delta H_{integrated} \cdot m_a$) is the enthalpy of the residual monomers polymerization, m_a is the employed sample mass in the DSC measurement and M_w is the molar mass of the monomer ($M_w^{EBPADMA} = 540$ g/mol). The ΔH_p corresponds to the integrated area, after subtracting the baseline and extracting the onset and offset temperature, as shown in **Supplementary Figure 4**. A conversion value of $94 \pm 2\%$ was calculated, *i.e.*, a value slightly higher than that found from Raman spectroscopy analysis.

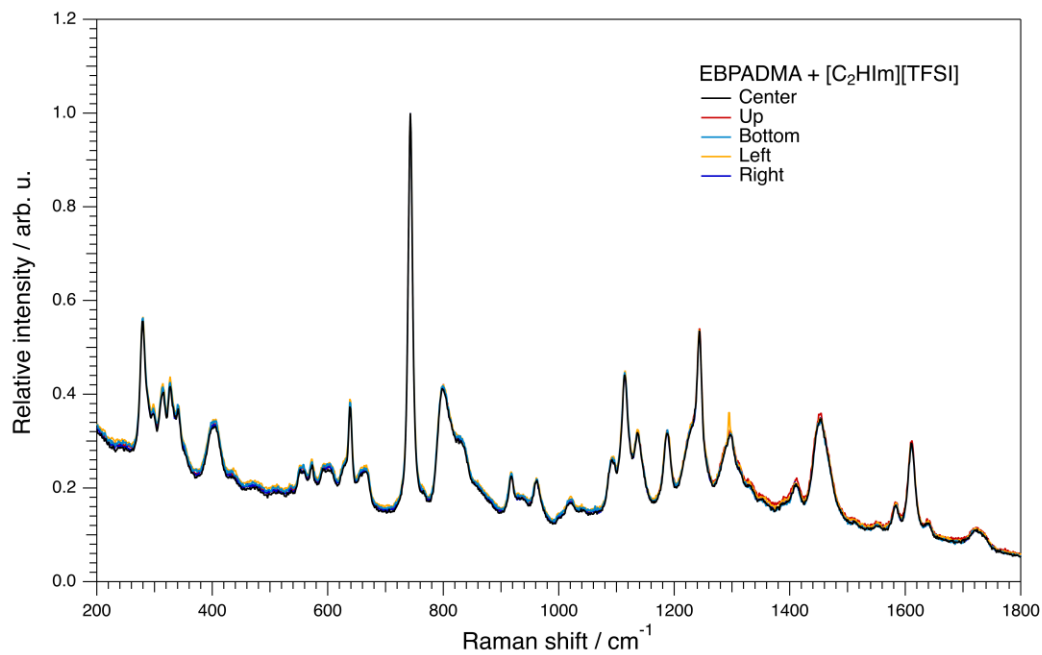


Supplementary Figure 4. DSC thermogram for EBPADMA+[C₂HIm][TFSI] at high temperatures, depicting the peak of residual monomers. The shadowed blue region corresponds to the integrated area, limited by the onset and offset temperatures.

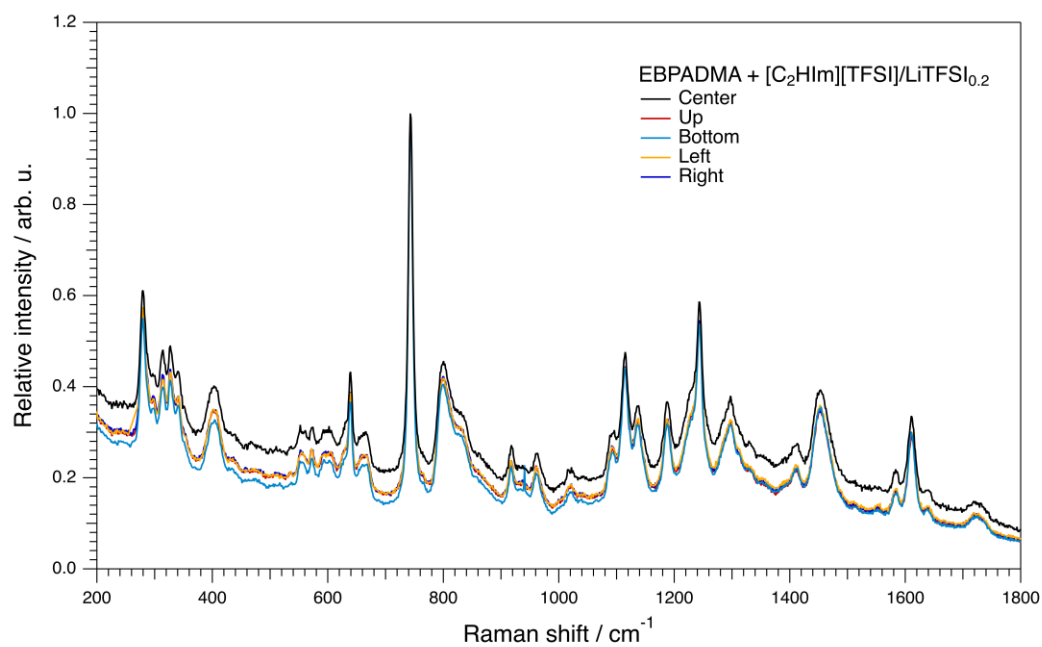
4. Raman spectroscopy data



Supplementary Figure 5. Selection of Raman spectra collected at room temperature along a line cross-sectioning the thickness of the EBPADMA+[C₂HIm][TFSI]/LiTFSI_{0.2} sample (see also Figure 6A of the main text).



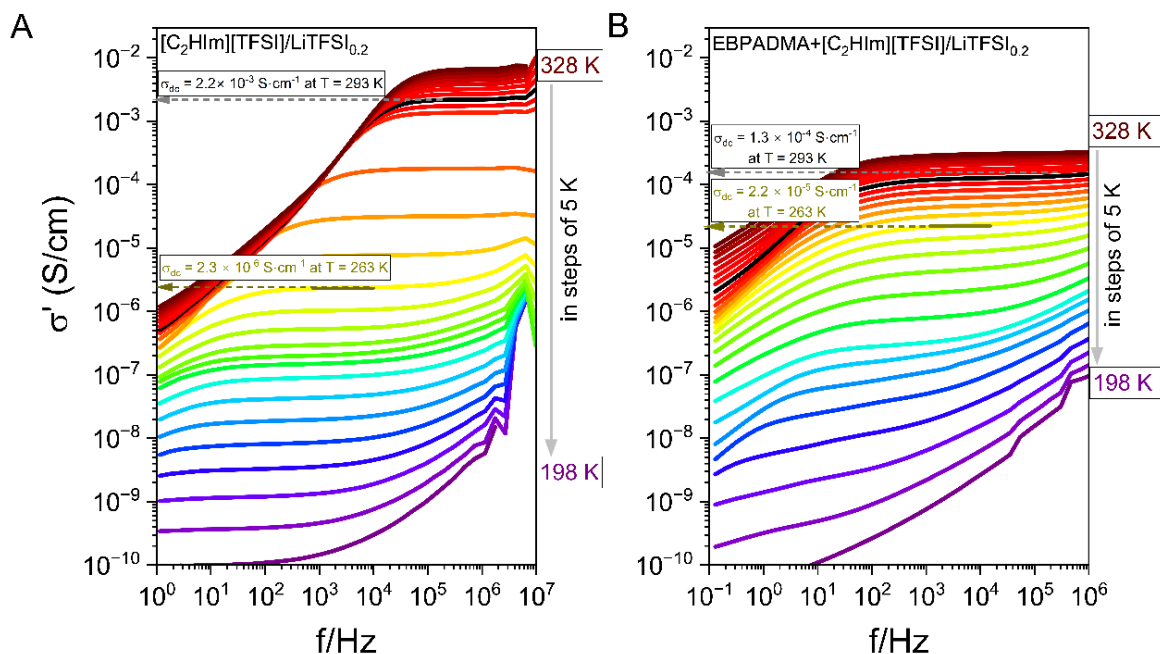
Supplementary Figure 6. Selection of Raman spectra collected at room temperature at arbitrarily selected spots on the bottom side of the EBPADMA+[C₂HIm][TFSI] sample.



Supplementary Figure 7. Selection of Raman spectra collected at room temperature at arbitrarily selected spots on the bottom side of the EBPADMA+[C₂HIm][TFSI]/LiTFSI_{0.2} sample.

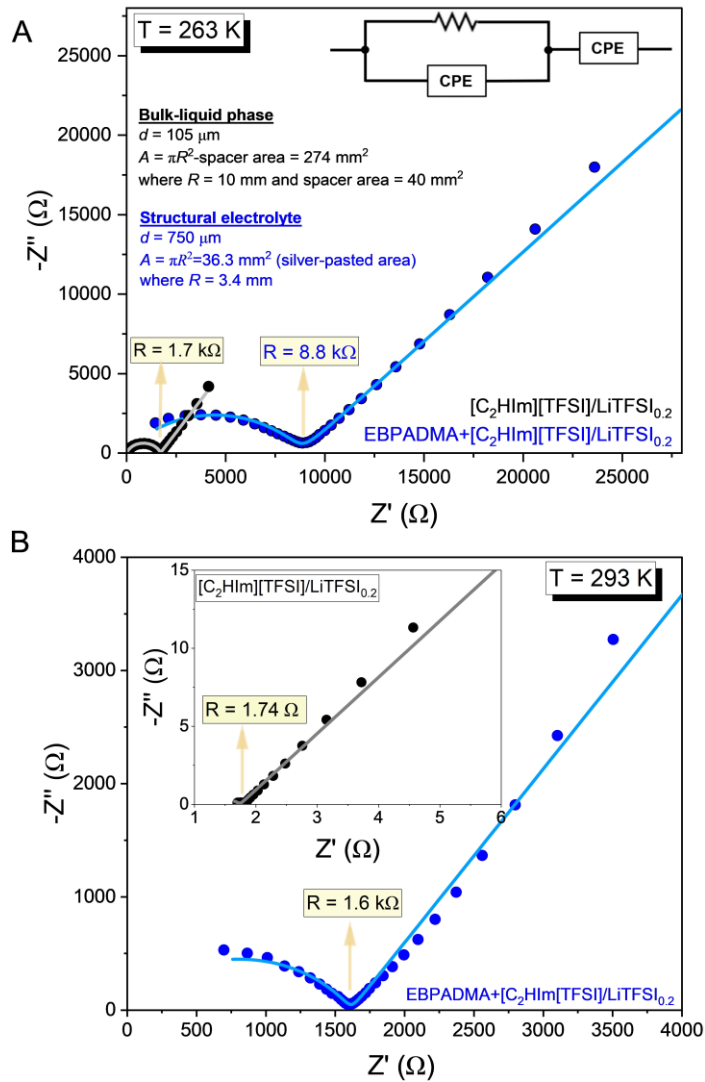
5. Dielectric spectroscopy data

The real part of the complex conductivity as a function of frequency is shown in **Supplementary Figure 8** for the EBPADMA+[C₂HIm][TFSI]/LiTFSI_{0.2} solid electrolyte and its respective bulk liquid electrolyte, for the selected temperature range between 198 and 328 K.



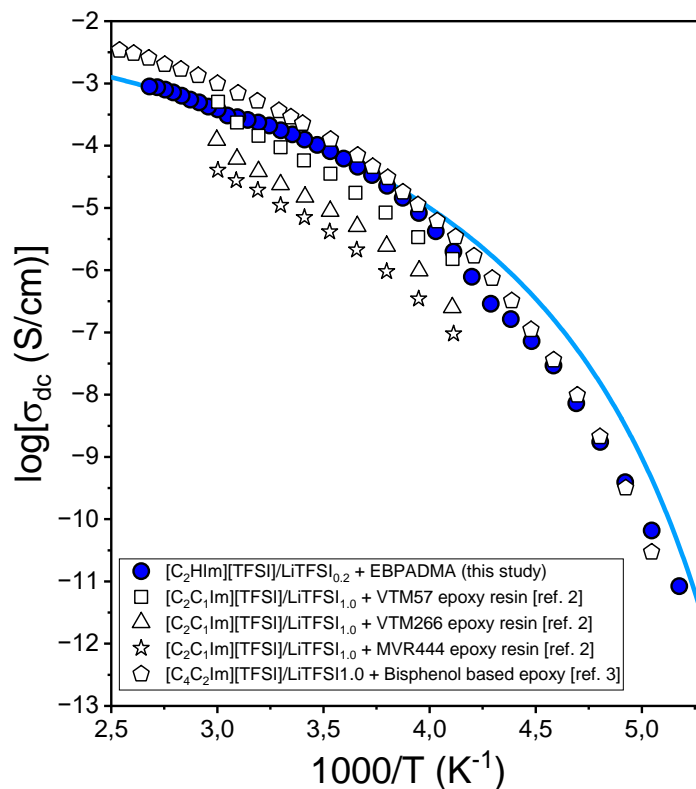
Supplementary Figure 8 Frequency-dependence of the real part of the complex conductivity for (A) [C₂HIm][TFSI] and (B) EBPADMA+[C₂HIm][TFSI]/LiTFSI_{0.2} in the temperature range 198 – 328 K, in steps of 5 K.

An alternative way for extracting the value of dc-conductivity is through the Nyquist plot, as shown in **Supplementary Figure 9**. The Nyquist plot exhibits a semicircle at higher frequencies and a capacitive tail at lower frequencies, as anticipated for exclusively ion-conducting electrolytes. The ionic conductivity can be calculated as follows: $\sigma_{dc} = d/R \cdot A$, where d is the sample thickness and A is the electrolyte area between the lower and upper electrode and R is the resistance, extracted from fitting with an equivalent circuit (see inset of **Supplementary Figure 9**).



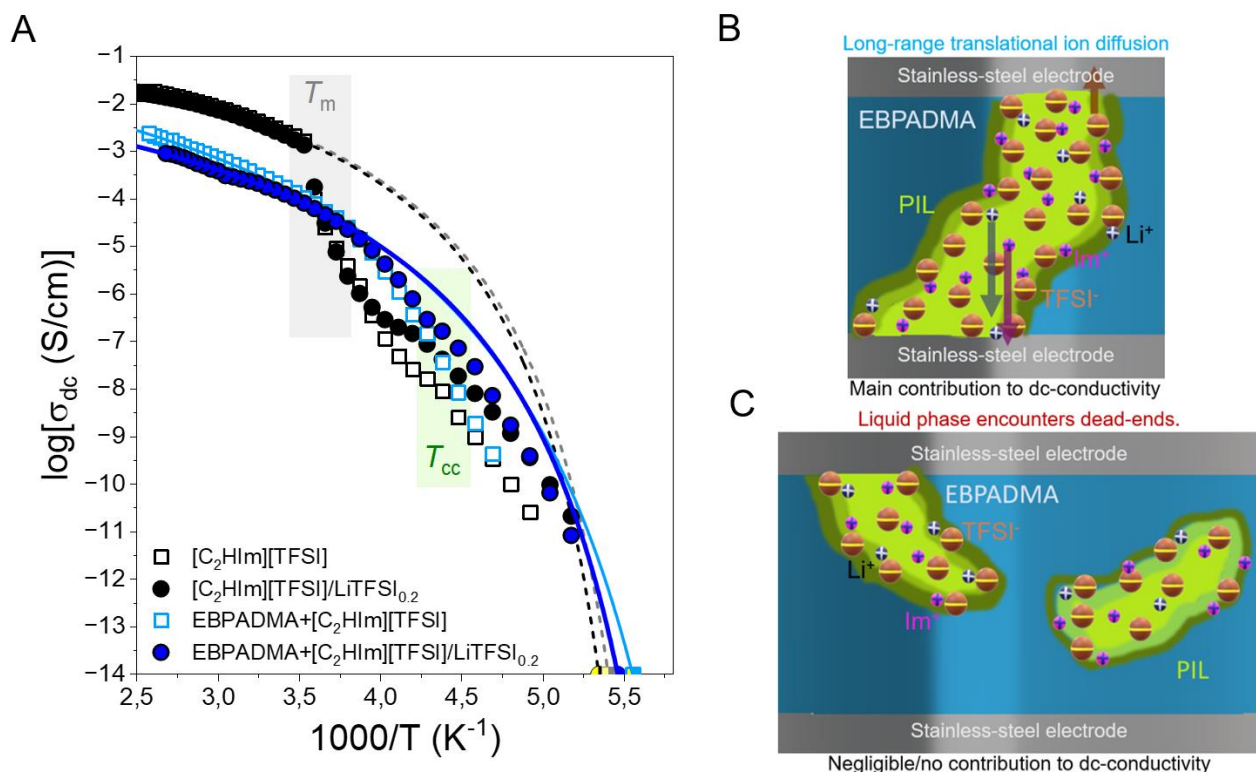
Supplementary Figure 9. Nyquist plot at (A) 263 K and (B) 293 K for the methacrylate based solid polymer electrolyte (blue symbols) doped with LiTFSI at a Li salt concentration of 0.2 m and the respective bulk liquid phase (black symbols), for frequencies in the range from 2.7 Hz to 8 MHz. The solid lines represent fits by the equivalent circuit, shown in the inset of Figure A. In Figure B, the Nyquist plot of the bulk liquid phase is shown in the inset for frequencies in the range from 750 Hz to 7 MHz. The extracted values of resistances and the geometrical characteristics required for the calculation of dc-conductivity are also included.

Supplementary Figure 10 provides a comparison between the temperature dependence of dc-conductivity measured in this study with that of similar systems reported in the literature.



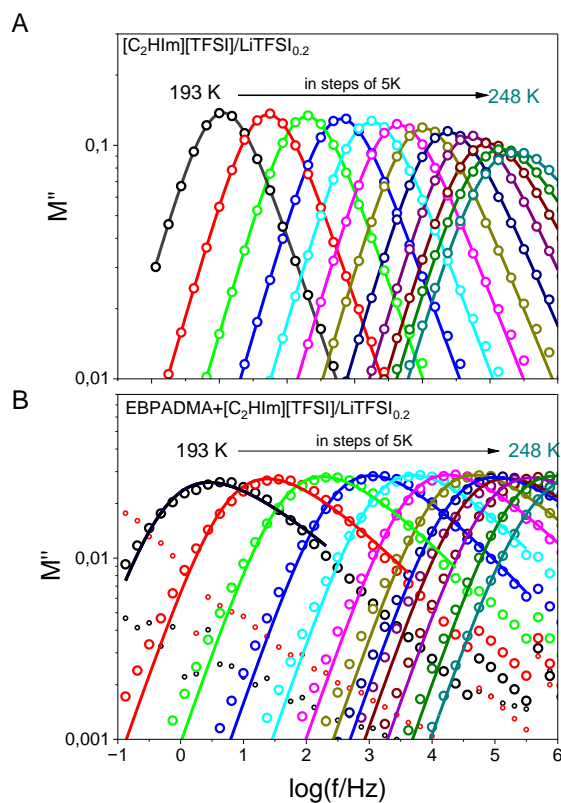
Supplementary Figure 10. Dc-conductivity as a function of inverse temperature for the EBPADMA+ $[\text{C}_2\text{HIm}][\text{TFSI}]/\text{LiTFSI}_{0.2}$ (solid blue symbols) solid electrolyte in comparison with the ionic conductivity data reported for epoxy resin-based solid electrolytes combined with the aprotic ionic liquids $[\text{C}_2\text{C}_1\text{Im}][\text{TFSI}]/\text{LiTFSI}$ (black symbols) reproduced from ref [2], and $[\text{C}_4\text{C}_2\text{Im}][\text{TFSI}]/\text{LiTFSI}$ (at 1M, dark-yellow symbols) reproduced from ref [3].

The temperature dependence of the dc-conductivity for the solid electrolytes and their respective bulk liquid electrolytes is provided in **Supplementary Figure 11A**. The results show that the SBEs exhibit about one order of magnitude lower conductivity than their corresponding bulk liquid phases. Moreover, **Supplementary Figures 11 (B, C)** show illustrations of a possible long-range translational ion diffusion contributing to the ionic conductivity and of the presence of non-percolating pores that impede ion transport. The conductivity data above the melting temperature were fitted by eq. 2, and the VFT parameters are provided in Table 2 of the main paper.

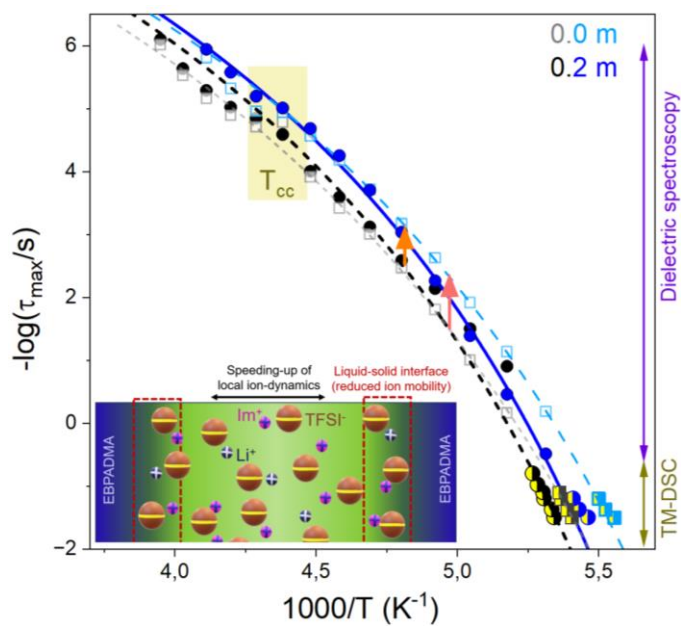


Supplementary Figure 11. (A) Temperature-dependence of the dc-conductivity for the studied electrolytes; EBPADMA+[C₂HIm][TFSI] (cyan open symbols) and EBPADMA+[C₂HIm][TFSI]/LiTFSI_{0.2} (blue solid symbols) in comparison with their respective bulk liquid electrolytes; [C₂HIm][TFSI] (black open symbols) and [C₂HIm][TFSI]/LiTFSI_{0.2} (filled black symbols), upon heating. The respective solid and dashed lines represent fits by eq. 2 for the solid electrolytes (solid lines) and their respective bulk liquid electrolytes (dashed lines). The shadowed green and grey areas mark the cold-crystallization and melting region, respectively. An illustration of (B) a possible long-range translational ion diffusion and (C) non-percolating pores that impedes the migration of ions between the two electrodes.

Relaxation dynamics and representative fitting curves of the σ -process for the SBE doped with LiTFSI and the corresponding bulk liquid electrolyte are shown in **Supplementary Figure 12**.



Supplementary Figure 12. Representative dielectric spectra of the electric modulus for (A) $[\text{C}_2\text{HIm}][\text{TFSI}]/\text{LiTFSI}_{0.2}$ and (B) $\text{EBPADMA}+[\text{C}_2\text{HIm}][\text{TFSI}]/\text{LiTFSI}_{0.2}$. The solid lines represent fits by eq. 4 as given in the main paper.



Supplementary Figure 13. Relaxation map showing the σ -process and the relaxation times of the structural α -process extracted from TM-DSC (symbols in yellow), for the $[\text{C}_2\text{HIm}][\text{TFSI}]$ (grey symbols), $[\text{C}_2\text{HIm}][\text{TFSI}]/\text{LiTFSI}_{0.2}$ (black

symbols), EBPADMA+[C₂HIm][TFSI] (cyan symbols) and EBPADMA+[C₂HIm][TFSI]/LiTFSI_{0.2} (blue symbols). The solid and dashed lines represent fits by the VFT equation (eq. 5) to the temperature dependence of the σ -relaxation of the solid electrolytes and their respective bulk protic ionic liquids. The colored area marks the cold-crystallization region. The inset shows an illustration about the gradient of viscosity that most likely takes place between the solid and liquid phases. The green (blue) color indicates the region with the lower (higher) effective medium's viscosity. The interfacial region between the two segregated phases is also indicated.

As shown in **Supplementary Figures 12 and 13**, SBEs exhibit faster ion dynamics, broadening of relaxation times and reduced dielectric strength as compared to the bulk liquid electrolytes, reflecting the impact of geometrical confinement. Different degrees of coupling between the structural relaxation and σ -process were evidenced in the undoped and LiTFSI-doped electrolytes.

REFERENCES

1. Alarcon RT, Gaglieri C, Rossi de Oliveira A, Bannach G. Use of DSC in Degree of Conversion of Dimethacrylate Polymers: Easier and Faster than MIR Technique. *Journal of Thermal Analysis and Calorimetry* 2018;132:1423-1427. **DOI:10.1007/s10973-018-6988-2**
2. Shirshova N, Bismarck A, Carreyette S. et al. Structural Supercapacitor Electrolytes Based on Bicontinuous Ionic Liquid-Epoxy Resin Systems. *J. Mater. Chem. A* 2013;1:15300-15309. **DOI: 10.1039/C3TA13163G**
3. Kwon SJ, Kim T, Jung BM, Lee SB, Choi UH. Multifunctional Epoxy-Based Solid Polymer Electrolytes for Solid-State Supercapacitors. *ACS Appl. Mater. Interfaces* 2018;10:35108-35117. **DOI: 10.1021/acsami.8b11016**